High Power Laser Science and Engineering, (2023), Vol. 11, e81, 8 pages.
doi:10.1017/hpl.2023.62

HIGH POWER LASER SCIENCE AND ENGINEERING

RESEARCH ARTICLE

High-energy and high-peak-power GHz burst-mode all-fiber laser with a uniform envelope and tunable intra-burst pulses

Shuailin Liu[1,2,3], Bin Zhang[1,2,3], Yuanzhuang Bu[1,2,3], Desheng Zhao[1,2,3], Xiran Zhu[1,2,3], Linyong Yang[1,2,3], and Jing Hou[1,2,3]

[1] *College of Advanced Interdisciplinary Studies, National University of Defense Technology, Changsha, China*

[2] *Nanhu Laser Laboratory, National University of Defense Technology, Changsha, China*

[3] *Hunan Provincial Key Laboratory of High Energy Laser Technology, Changsha, China*

(Received 26 April 2023; revised 27 June 2023; accepted 25 July 2023)

Abstract

We report a Yb-doped all-fiber laser system generating burst-mode pulses with high energy and high peak power at a GHz intra-burst repetition rate. To acquire the uniform burst envelope, a double-pre-compensation structure with an arbitrary waveform laser diode driver and an acoustic optical modulator is utilized for the first time. The synchronous pumping is utilized for the system to reduce the burst repetition rate to 100 Hz and suppress the amplified spontaneous emission effect. By adjusting the gain of every stage, uniform envelopes with different output energies can be easily obtained. The intra-burst repetition rate can be tuned from 0.5 to 10 GHz actively modulated by an electro-optic modulator. Optimized by timing control of eight channels of analog signal and amplified by seven stages of Yb-doped fiber amplifier, the pulse energy achieves 13.3 mJ at 0.5 ns intra-burst pulse duration, and the maximum peak power reaches approximately 3.6 MW at 48 ps intra-burst pulse duration. To the best of our knowledge, for reported burst-mode all-fiber lasers, this is a record for output energy and peak power with nanosecond-level burst duration, and the widest tuning range of the intra-burst repetition rate. In particular, this flexibly tunable burst-mode laser system can be directly applied to generate high-power frequency-tunable microwaves.

Keywords: burst-mode laser; fiber laser; high peak power; high pulse energy

1. Introduction

Burst-mode lasers generate a string of closely spaced short pulses in a lower repetition, achieving high repetition rate and high peak power simultaneously. Some applications of high-energy and high-peak-power burst-mode lasers include materials processing[1–6], precision surgery[7–9], high-resolution detection[10–12], high-power microwave generation[13], and so on. A novel application in recent years for burst-mode lasers is high-power pulsed agile microwave generation. A few studies have reported on a pulsed laser illuminating a photoconductive semiconductor switch (PCSS) to generate a narrowband microwave that possesses the identical waveform of the laser pulses[14–16]. The frequency spectrum and peak power of the microwave depend on that of the laser pulse. In particular, a laser working in the burst-mode is beneficial to generate high-frequency (over GHz level), high-power and agile frequency microwave burst signals, for which some output characteristics need to be considered. For one thing, the even distribution of the burst envelope affects the effective microwave burst duration. For another, the intra-burst repetition rate needs to be tuned flexibly to yield a frequency-adjustable microwave signal. Therefore, an approximate uniform envelope and tunable frequency for the burst-mode laser are required.

In 2021, we demonstrated that, for the first time, a uniform envelope burst-mode fiber laser system can be employed to generate a narrowband microwave with tunable frequency (0.80–1.12 GHz) by illuminating a linear-state PCSS[13]. To compensate for the envelope distortion

Correspondence to: Bin Zhang and Jing Hou, College of Advanced Interdisciplinary Studies, National University of Defense Technology, Changsha 410073, China. Emails: nudtzhb@163.com (B. Zhang); houjing25@sina.com (J. Hou)

caused by the gain saturation effect, pre-compensation envelope shaping according to the inverse Frantz–Nodvik equation[17,18] is realized. The pulse energy and peak power of the laser are 200 μJ and 4 kW, respectively, and the generated microwave power is 300 W. However, if the laser peak power was further promoted for higher microwave power output, the envelope would suffer more severe waveform distortion due to the larger gain of the front edge. In the same year, a 4 mJ burst-mode laser system was constructed based on a fiber–solid hybrid structure, whose burst repetition rate was reduced to 100 Hz and peak power reached 80 kW[19]. On the one hand, the free-space configuration for the solid-state laser amplifier occupies enormous space and is inconvenient for practical application. On the other hand, the reliability and stability of solid laser amplifiers are inferior to those of fiber laser amplifiers. Therefore, the all-fiber structure and a new scheme for the higher-power pulse pre-compensation have become the development directions of the burst-mode laser for high-power microwave generation.

Moreover, to adapt burst-mode lasers for other different application requirements, in addition to increasing the burst energy and peak power, it is necessary to promote the tuning performance in the time domain, including the repetition rate and duration of the intra-burst pulse. As we know, there are four implementation constructions for the reported high-energy/high-peak-power burst-mode fiber lasers. The first is to employ a mode-locked fiber laser modulated by an acoustic optical modulator (AOM) periodically cutting off pulse train[20,21]. The second is to utilize the pulse fiber multiplier to achieve a high repetition rate of the intra-burst pulse[22–24]. However, these two methods are unable to flexibly adjust the repetition rate of the intra-burst pulse. Direct seed shaping technology is convenient to generate an arbitrarily tunable burst-mode pulse, which is the third method[25], but is limited by circuit performance: this method could only generate an intra-burst pulse at the μs–ns level. The fourth method is to use an electro-optical modulator (EOM) to modulate at a very fast rate[13,26], which could achieve the widest tuning range of ps–ns pulse duration and an over-GHz repetition rate, in theory. However, because of high insertion loss and the single-mode fiber input, it is difficult to amplify the weak signals from the EOM while maintaining the uniformity of the envelope. There is no report to realize such a high-energy burst-mode fiber laser.

In this report, we demonstrate a high-pulse-energy and high-peak-power all-fiber burst-mode laser system whose repetition rate and duration of the intra-burst pulse are tunable. To achieve a burst envelope that is approximately uniform in the seven stages of the fiber amplifier, we promote a new scheme for pre-compensation combining an arbitrary waveform laser diode (LD) driver and an AOM, which is called a double-pre-compensation structure. The laser system can deliver burst-mode pulses with frequency of 0.5–10 GHz that are tunable and intra-burst pulse duration of 48 ps–0.5 ns that is tunable. Meanwhile, we construct a multiplex synchronous timing system to realize the synchronous pumping for every stage of the amplifier. At the main amplifier, a 100 μm core diameter gain fiber is utilized to acquire the higher energy and reduce the nonlinear effect, so the highest energy of 13.3 mJ and the highest peak power of approximately 3.6 MW for a burst-mode pulse are achieved. This laser system is useful for high-power microwave generation and other potential applications.

2. Experimental setup

A schematic diagram of the laser system setup is depicted in Figure 1(a). The laser system is mainly segmented into five parts: a pulsed seed, three stages of single-mode pre-amplifier, a high-repetition-rate modulation part, a secondary pre-compensation modulation part and four stages of multi-mode amplifier. The seed laser is a 1064 nm Fabry–Pérot (FP) LD with peak power of 1 W and 3 dB bandwidth of approximately 2 nm. One arbitrary waveform LD driver is utilized to directly modulate the seed LD into the pre-compensated waveform with the repetition rate of 100 Hz.

There are three stages for the single-mode pre-amplifiers, whose gain media are all highly doped single-mode Yb^{3+}-doped fibers (YDFs) with the absorption coefficient of 250 dB/m at 976 nm and pump sources are single-mode 976 nm LDs. The high-repetition-rate modulation part includes an EOM with bandwidth of 10 GHz and an arbitrary waveform generator (AWG-1, Keysight M8195A) generating a high-speed electric signal with 45 GHz bandwidth. The secondary pre-compensation modulation part includes an AOM with bandwidth of 200 MHz and AWG-2 exporting the pre-compensation waveform. The AOM not only reforms the pulse shape to the pre-compensation waveform, but also blocks the amplified spontaneous emission (ASE) pedestal from the pre-amplifiers in the time domain. It is worth noting that the third stage of the single-mode pre-amplifier is positioned after the EOM and before the AOM. This stage of the amplifier makes up the insertion loss and modulation of the EOM and provides the relatively high initial energy for the secondary pre-compensation of the AOM. An isolator/bandpass filter (IBP) with the 3 dB bandwidth of 2 nm is placed after the AOM. The multi-mode amplifiers in the system consist of four all-fiber double-clad amplifier stages, which are shown as the fourth to seventh amplifiers in Figure 1. The fourth amplifier employs a 3 m 15/130 μm double-clad YDF (DCYDF) with the absorption coefficient of 5.4 dB/m at 976 nm, and an isolator (ISO) is employed to avoid the backward reflections of the following amplifiers. The fifth amplifier uses a 2.5 m 30/250 μm DCYDF with the absorption coefficient of 7.5 dB/m at 976 nm. The sixth amplifier uses a 2.8 m 48/400 μm DCYDF with the absorption coefficient of 7.5 dB/m at 976 nm. The main amplifier employs a 1.8 m 100/400 μm DCYDF with

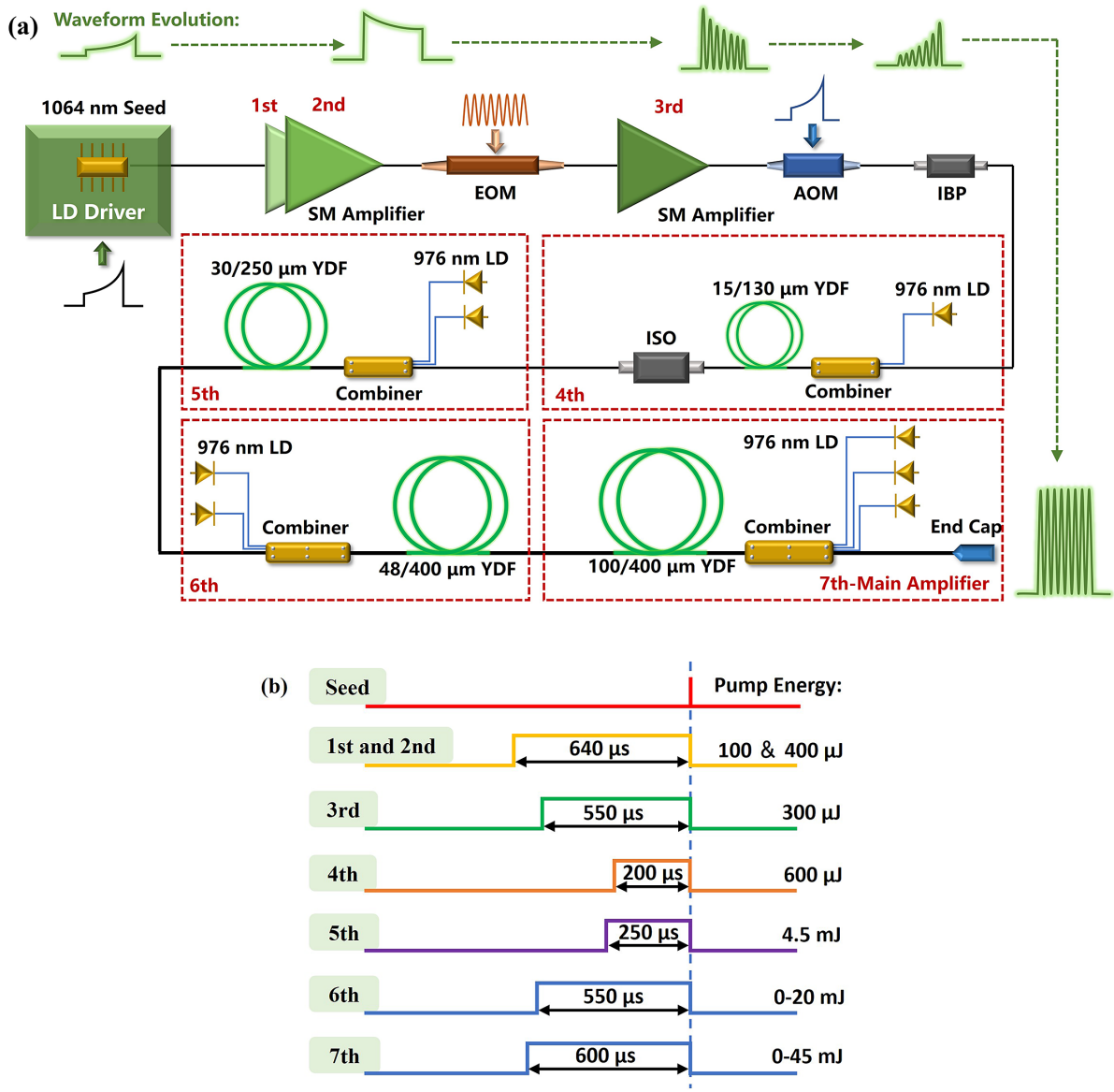

Figure 1. (a) Schematic diagram of the laser system. LD, laser diode; IBP, isolator/bandpass filter hybrid; SM, single mode; YDF, Yb^{3+}-doped fiber; AOM, acousto-optic modulator; ISO, isolator. (b) Time sequence of seed and pump pulses.

the absorption coefficient of 22.5 dB/m at 976 nm. Moreover, a 400 μm coreless fiber is spliced as the end cap at the end of the main amplifier to avoid damage to the output end face.

In order to realize synchronous pumping and the secondary pre-compensation technique, a multiplex synchronous timing system is employed to the seed, AOM and every stage of the amplifier in the laser system[27]. There is rather low repetition rate (100 Hz) for the signal and pump pulse so that the system operates at a relatively low average power level. Therefore, the amplifiers are free of cooling, and the volume required for the whole system is greatly compressed. The time sequence of the seed and pump pulses is illustrated in Figure 1(b). Considering the burst energy, fiber parameters and the peak power that pump LDs could supply, the pump energy and width in every stage are optimized in experiments to suppress ASE and the nonlinear effect. The seed pulse arrives at the end of the pump pulse, so that the stored particle in the upper level by pumping is consumed, and the extraction of stored energy by ASE is reduced. It should be noted that the last two stages of pump energies need to be adjusted for the tunable output parameters.

The green waveforms and arrows in Figure 1(a) depict the waveform evolution of a 100 Hz laser pulse from seed to output. First, a pre-compensation pulse waveform is loaded to the LD seed driver. Second, two stages of pre-amplifier promote the pulse energy and bring about the waveform distortion at the same time. Third, GHz modulation is loaded to the pulses by the EOM and the pulses are modulated into burst-mode pulses. After the third stage of the pre-amplifier,

the AOM shapes the burst, which presents distortion of the low front and high back caused by the gain saturation effect from the pre-amplifiers to the pre-compensation waveform. Finally, four stages of multi-mode amplifier boost the pulse energy to approximately mJ level and the output burst waveform is distributed approximately uniformly.

The temporal laser pulse train and radiofrequency (RF) spectrum are monitored by a 36 GHz high-speed digital oscilloscope (Lecroy, LM-10-35-ZI), connected with a 45 GHz InGaAs photodetector. The optical spectrum is detected by an optical spectrum analyzer (Yokogawa, AQ6370). Two pyroelectric energy meters (Ophir PE9-ES-C and PE50-DIF-C) are employed to detect relatively low (<100 μJ) and high (>100 μJ) pulse energy, respectively.

3. Results and discussion

In the experiment, the laser system is investigated in detail first at a 1-GHz repetition rate and 50% intra-burst duty cycle. As for the seed, to make it more convenient for seed pulse amplification and leave leeway for the secondary pre-compensation, the seed pulse duration is longer than that of the output burst, which is set to approximately 70 ns. The laser system is divided into two parts, the first three single-mode amplifiers and the last four multi-mode amplifiers, to calculate the pre-compensation. According to the inverse Frantz–Nodvik equation, two pre-compensation waveforms are calculated as shown in Figure 2. The electrical signal waveform for the seed driver (blue line) and the pulse train of the seed (red line) are depicted in Figure 2(a). A pre-compensated envelope for the seed is loaded to the LD seed driver. The pulse duration of the seed is approximately 70 ns, which is longer than that of the waveform because of ascending and descending time for electrical modulation. The blue line and red line in Figure 2(b) illustrate the pre-compensation waveform from the AWG signal and the burst-mode pulse waveform after AOM modulation, respectively. The envelope of the burst-mode pulse generally resembles the pre-compensated waveform. Here, we obtain the pre-compensated burst-mode seed with a burst duration of approximately 60 ns.

The burst-mode seed is introduced into four stages of the multi-mode amplifier to enhance the pulse energy. Figure 3(a) shows the pulse energy changing with the pump energy of the main amplifier, which manifests the slope efficiency of 46.96%. The maximum pulse energy achieves 13.3 mJ, which is the highest energy for an all-fiber GHz burst-mode pulse to our knowledge, and the calculated highest peak power reaches approximately 0.53 MW. The extraction efficiency is 31.4% at the maximum energy. The temporal shape evolution of the burst-mode pulse after the main amplifier is shown in Figure 3(b). The front part of the burst envelope lifts with the pump power increasing on account of the gain saturation effect, and the approximately uniform envelope is achieved at the maximum output energy, which indicates that the gain saturation effect is mitigated successfully by secondary pre-compensation. Because of the relatively slow rising and falling time of AOM modulation (~10 ns), it is unable to achieve a rapid edge for both sides of envelope. Figure 3(c) depicts the local intra-burst pulse and the setup signal in detail, showing a stable format for the intra-burst pulse. The amplified intra-burst pulse stays at approximately 0.5 ns. As shown in Figure 3(d), the spectrum of the output laser broadens gradually with the increase of pulse energy, mostly resulting from self-phase modulation. At the maximum output energy, the 3 and 20 dB bandwidths are respectively 7.8 and 42.6 nm. However, the ASE component gradually grows in the 1.03 μm band when the energy increases to over approximately 3 mJ and the intensity difference of the signal peak and ASE spectrum is approximately 30 dB at the maximum energy. If the pump energy is further increased, the self-stimulation effect would occur, which could damage the laser system. Therefore, the enhancement of burst-mode pulse energy is mainly limited by ASE.

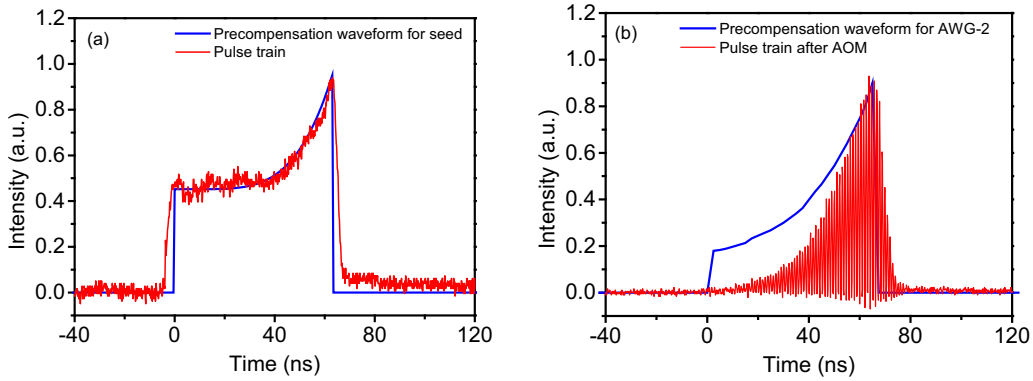

Figure 2. Evolution of the pulse shape during the secondary pre-compensation process. (a) The signal waveform for the seed driver and the pulse train of the seed. (b) The signal waveform from the AWG and the burst-mode pulse waveform after AOM modulation.

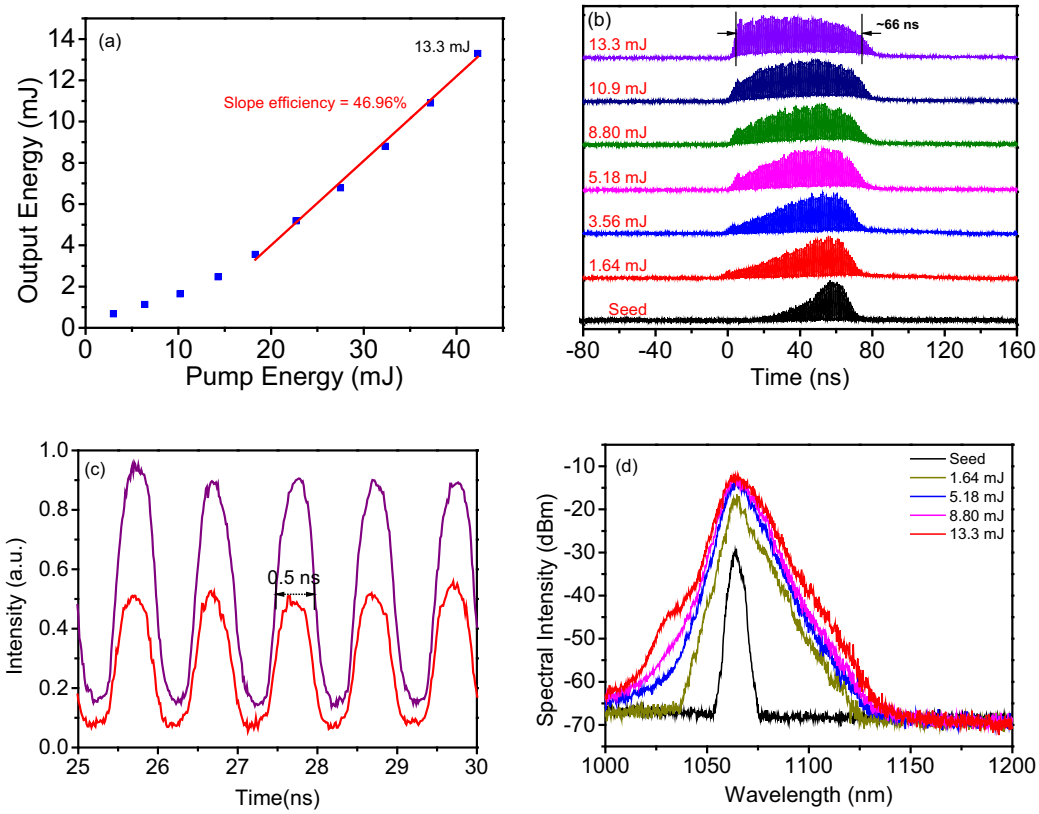

Figure 3. Performance of the output burst-mode laser. (a) Variation of pulse energy with different pump energies of the main amplifier. (b) Temporal shape of the pulse with different pulse energies. (c) Comparison of the intra-burst pulse in detail between the seed and output. (d) Spectrum evolution of the seed and main amplifier.

We have noticed that there are different degrees of waveform distortion to the burst-mode pulse for each amplifier because of the variant gain saturation effect brought about by different types of YDF. Therefore, the burst envelope can remain approximately uniform at different pulse energies by adjusting the pump power of each stage of the amplifier.

To study the uniformity of the burst envelope, we define an envelope uniformity factor as a relative standard deviation (RSD) of the peak power in a burst, which is presented as follows:

$$U = \frac{1}{P_{\mathrm{Avg}}}\sqrt{\frac{\sum_{i=1}^{n}\left(P_i - P_{\mathrm{Avg}}\right)^2}{n}} \times 100\%, \qquad (1)$$

where U represents the uniformity factor; n is the intra-burst pulse number in the calculation region of a burst; P_i and P_{Avg} are the peak power of every intra-burst pulse and the

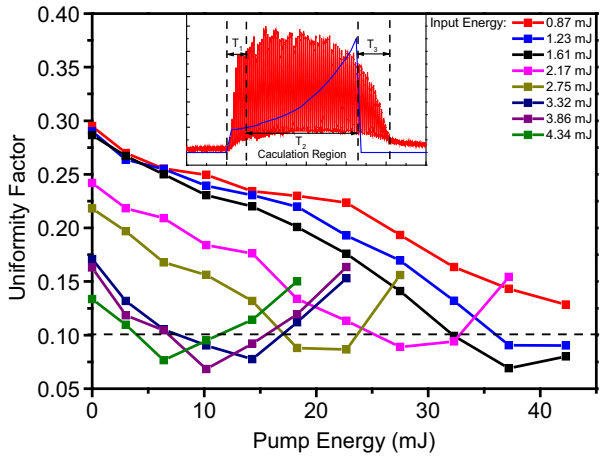

Figure 4. The envelope uniformity factors with different input energies as a function of main amplifier pump energy. Inset: diagram of the calculation region of the envelope uniformity factor.

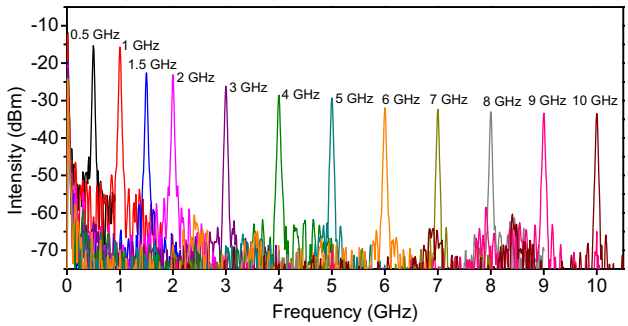

Figure 5. RF spectrum of different frequencies ranging from 0.5 to 10 GHz.

average peak power, respectively. It is worth noting that the bandwidth limitation of the AOM leads to an approximately 10 ns rising and falling time of AOM modulation. As shown in the inset of Figure 4, the rising edge of the burst is a 10 ns period from the beginning of the modulation signal (T_1), and the falling edge of the burst is the optical modulation time after the end of the AWG signal (T_3), which are both excluded from the calculation. In other words, the calculation region of the envelope uniformity factor is from the moment 10 ns after the start of the modulation signal to the moment when the modulation signal ends (T_2). The burst-mode pulse can be regarded as relatively uniform if $U < 10\%$. Figure 4 shows the dependence of the uniformity factor with different input energies of the main amplifier on pump energy. We can clearly see that the uniformity factor declines with the input energy increasing from 0.87 to 4.34 mJ when there is no pump energy of the main amplifier. In this condition, the rising amplitude of the envelope of a burst is maintained for the relatively small gain of the front stage. With the enhancement of pump energy, the uniformity factor generally decreases and then increases. When the leading edge of the envelope is amplified to be basically flush with the trailing edge, the uniformity factor reaches the lowest point. Further injecting pump energy leads to a higher leading edge than trailing edge and the increase of the uniformity factor. The higher input energy injected, the less pump energy required to achieve a relatively uniform envelope, and the corresponding output energy is lower. Besides, a similar situation is found in the sixth amplifier. It is not described in this paper to avoid repetition. Thus, uniform envelopes with different output energies can be easily obtained by adjusting the pump power of every stage of the amplifier without resetting the pre-compensation waveform. Compared with setting the pre-compensation envelope by multiple calculations[18,26,28], this method is unable to obtain an optimal envelope, but it is more convenient and faster to achieve an approximately uniform envelope.

By changing the parameters of AWG-1, the repetition rate and intra-burst duty cycle can be adjusted conveniently. As shown in Figure 5, the intra-burst repetition rate is tuned from 0.5 to 10 GHz. The fundamental to harmonic frequency ratios are all over 30 dB. This is the widest tuning range of the intra-burst repetition rate for reported burst-mode fiber lasers. Figure 6 compares the output performance under different intra-burst duty cycles of 5%, 10%, 25% and 50% at the same pump energy of the main amplifier (42.3 mJ) in detail when the repetition rate is fixed at 1 GHz. The energies and peak powers of different burst-mode pulses are shown in Figure 6(a). As can be observed, with the increase of the intra-burst duty cycle, the output energy is elevated from 9.3 to 13.3 mJ. The extraction efficiency and duty cycle show a positive correlation at the same pump energy. However, the peak power is significantly enhanced, because the total energy is distributed to the shorter burst duration, leading

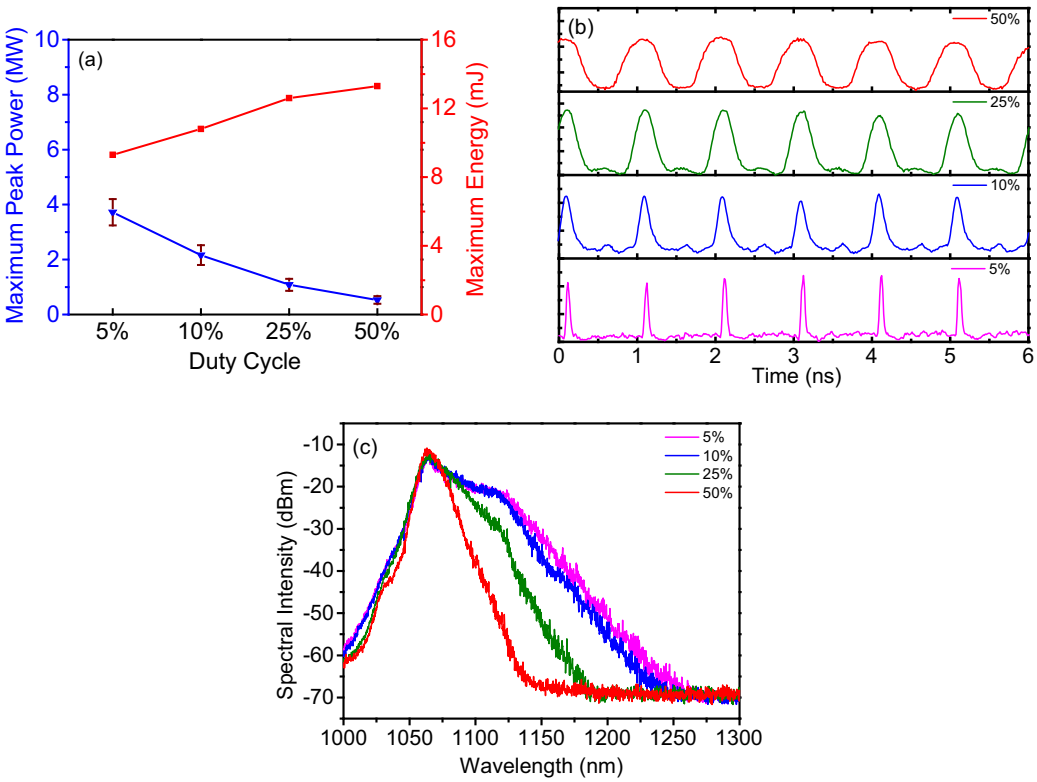

Figure 6. Performance of the output under different intra-burst duty cycles at the same pump energy (42.3 mJ) when the intra-burst repetition rate is fixed at 1 GHz. (a) The energy and peak power. (b) The waveform details of the intra-burst pulse. (c) The spectra in the 300 nm scanning range.

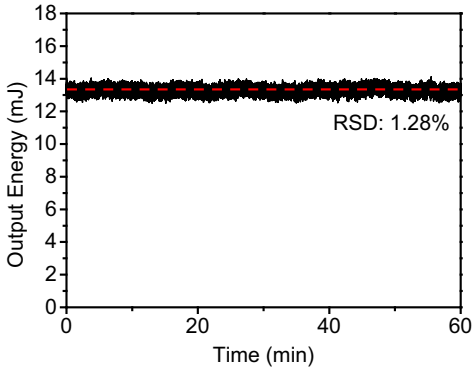

Figure 7. The long-term stability of energy, measured at an output energy of 13.3 mJ (50 ns, 1 GHz).

to higher peak power. It is remarkable that the highest peak power reaches approximately 3.6 MW at the 5% intra-burst duty cycle, which breaks the peak power record for GHz burst-mode all-fiber lasers. Figure 6(b) illustrates a detailed comparison of intra-burst pulses. The intra-burst pulse widths of the four cases are about 0.5 ns, 0.24 ns, 96 ps and 48 ps, respectively. As can be seen in Figure 6(c), the spectrum broadened with the intra-burst duty cycle reduces. The nonlinear effect is stronger for the smaller intra-burst duty cycle due to the higher peak power. In fact, there is limitation of the intra-burst pulse parameters when using an EOM to form the burst. In this work, we employ an EOM with a 10 GHz bandwidth, so 10 GHz and approximately 48 ps are the highest repetition rate and the narrowest intra-burst pulse duration the laser system can reach, respectively. If we want to achieve a higher repetition rate and narrower intra-burst pulse duration, an EOM with higher bandwidth (20 or 40 GHz) should be utilized. Moreover, by re-editing the pre-compensation waveforms of the LD seed driver and AWG-2, an arbitrary envelope shape and tunable burst duration can be achieved.

To test the stability of the laser system, the burst-mode pulse energy is recorded for 60 minutes at the maximum output, as shown in Figure 7. The corresponding RSD of the energy fluctuation is 1.28%. The beam quality at the output of the laser is measured. The output beam quality factor (M^2) at the maximum output energy (13.3 mJ) is 9.05/8.98 in the x/y direction.

4. Conclusion

In conclusion, we have reported an all-fiber burst-mode laser system operating at a burst repetition rate of 100 Hz. In order to compensate for the intense gain saturation effect from the seven stages of the fiber amplifier, we propose a double-pre-compensation structure. A uniformly distributed burst-mode pulse with energy of 13.3 mJ and peak power of approximately 3.6 MW is achieved from a 100 μm core diameter fiber amplifier. The approximately uniform burst envelope can be obtained at different pulse energies by adjusting the pump energy at each stage. Moreover, the repetition rate and pulse duration of the intra-burst pulse can be tuned conveniently for adapting it to different applications, and the widest reported tuning range (0.5–10 GHz) for the intra-burst repetition rate is achieved.

Acknowledgements

This work was supported by the National Natural Science Foundation of China (No. 62205374) and the Research Funds of the State Key Laboratory of Pulsed Power Laser Technology, China (Nos. SKL2021KF07 and SKL2020ZR06). The authors are grateful to Jinmei Yao, Xiaoyong Xu, Sen Guo and Weide Hong for their assistance during the experiment.

References

1. C. Kerse, H. Kalaycıoğlu, P. Elahi, B. Çetin, D. K. Kesim, Ö. Akçaalan, S. Yavaş, M. D. Aşık, B. Öktem, H. Hoogland, R. Holzwarth, and F. Ö. Ilday, Nature **537**, 84 (2016).
2. S. Kawabata, S. Bai, K. Obata, G. Miyaji, and K. Sugioka, Int. J. Extrem. Manuf. **5**, 015004 (2023).
3. M. Domke, V. Matylitsky, and S. Stroj, Appl. Surf. Sci. **505**, 144594 (2019).
4. K. Mishchik, G. Bonamis, J. Qiao, J. Lopez, E. Audouard, E. Mottay, C. Honninger, and I. Manek-Honninger, Opt. Lett. **44**, 2193 (2019).
5. F. Paz-Buclatin, M. Esquivel-González, A. Casasnovas-Melián, O. de Varona, C. Cairós, J. M. Trujillo-Sevilla, K. Kamada, A. Yoshikawa, J. M. Rodríguez-Ramos, and L. L. Martin, Nanophotonics **12**, 1511 (2023).
6. J. J. Kočica, J. Mur, and J. Petelin, Opt. Express **29**, 22868 (2021).
7. R. S. Marjoribanks, C. Dille, J. E. Schoenly, L. McKinney, A. Mordovanakis, P. Kaifosh, P. Forrester, Z. Qian, A. Covarrubias, and Y. Feng, Photon. Lasers Med. **1**, 155 (2012).
8. P. Elahi, H. Kalaycıoğlu, Ö. Akçaalan, Ç. Şenel, and F. Ö. Ilday, Opt. Lett. **42**, 3808 (2017).
9. W. Yue, Y. Zhang, L. Shi, T. Chen, J. Chen, B. Wu, S. Zhang, R. Shu, and Y. Shen, Results Phys. **9**, 100309 (2022).
10. N. Ji, J. C. Magee, and E. Betzig, Nat. Methods **6**, 197 (2009).
11. L. Tan, W. Jing, G. I. Petrov, V. V. Yakovlev, and H. F. Zhang, Med. Phys. **37**, 1518 (2010).
12. O. Volodarsky, Y. Hazan, M. Nagli, and A. Rosenthal, Opt. Express **30**, 8959 (2022).
13. X. He, B. Zhang, S. Liu, L. Yang, J. Yao, Q. Wu, Y. Zhao, T. Xun, and J. Hou, High Power Laser Sci. Eng. **9**, e13 (2021).
14. Q. Wu, Y. Zhao, T. Xun, H. Yang, and W. Huang, IEEE Electron Device Lett. **40**, 1167 (2019).
15. J. Zhang, D. Zhang, Y. Fan, J. He, X. Ge, X. Zhang, J. Ju, and T. Xun, Phys. Plasmas **27**, 010501 (2020).
16. X. Chu, J. Liu, T. Xun, L. Wang, H. Yang, J. He, and J. Zhang, IEEE Trans. Electron Devices **69**, 597 (2022).
17. J. Petelin, B. Podobnik, and R. Petkovšek, Appl. Opt. **54**, 4629 (2015).
18. D. N. Schimpf, C. Ruchert, D. Nodop, J. Limpert, A. Tunnermann, and F. Salin, Opt. Express **16**, 17637 (2008).
19. X. He, B. Zhang, C. Guo, L. Yang, and J. Hou, IEEE Photon. J. **13**, 1501009 (2021).
20. H. Kalaycioglu, K. Eken, and F. Ö. Ilday, Opt. Lett. **36**, 3383 (2011).

21. H. Yang, Y. Chen, K. Ding, F. Jia, K. Li, and N. Copner, Appl. Phys. B **126**, 127 (2020).
22. C. Kerse, H. Kalaycıoğlu, P. Elahi, Ö. Akçaalan, and F. Ilday, Opt. Commun. **366**, 404 (2016).
23. J. Liu, X. Li, S. Zhang, M. Han, and Z. Yang, IEEE J. Sel. Top. Quantum Electron. **25**, 8900106 (2018).
24. T. Bartulevicius, K. Madeikis, L. Veselis, V. Petrauskiene, and A. Michailovas, Opt. Express **28**, 13059 (2020).
25. T. Chen, H. Liu, W. Kong, and R. Shu, Opt. Express **24**, 20963 (2016).
26. M. Nie, X. Cao, Q. Liu, E. Ji, and X. Fu, Opt. Express **25**, 13557 (2017).
27. M. Šajn, J. Petelin, V. Agrež, M. Vidmar, and R. Petkovšek, Opt. Laser Technol. **88**, 99 (2017).
28. M. Jiang, R. Su, P. Zhang, and P. Zhou, Laser Phys. Lett. **15**, 065101 (2018).